Applied Catalysis B: Environmental 180 (2016) 139–149

Contents lists available at ScienceDirect

Applied Catalysis B: Environmental

journal homepage: www.elsevier.com/locate/apcatb

Stabilized ordered-mesoporous Co_3O_4 structures using Al pillar for the superior CO hydrogenation activity to hydrocarbons

Chang-Il Ahn [a], Hyun Mo Koo [a], Jae Min Jo [a], Hyun-Seog Roh [b], Jong-Bae Lee [c], Yun-Jo Lee [c], Eun Joo Jang [d], Jong Wook Bae [a,*]

[a] School of Chemical Engineering, Sungkyunkwan University (SKKU), Suwon, Gyeonggi-do 440-746, Republic of Korea
[b] Department of Environmental Engineering, Yonsei University, 1 Yonseidae-gil, Wonju, Gangwon 220-710, Republic of Korea
[c] Alternative Chemicals/Fuel Research Center, Korea Research Institute of Chemical Technology (KRICT), P.O. Box 107, Yusong, Daejon 305-600, Republic of Korea
[d] Material Research & Development Center, Samsung Advanced Institute of Technology (SAIT), Suwon, Gyeonggi-do 449-901, Republic of Korea

ARTICLE INFO

Article history:
Received 6 February 2015
Received in revised form 8 May 2015
Accepted 15 June 2015
Available online 18 June 2015

Keywords:
Fischer–Tropsch synthesis
Ordered-mesoporous Co_3O_4
Al_2O_3 pillar
Structural stability
Mesoporous channel reactor

ABSTRACT

The metal oxide pillared ordered-mesoporous Co_3O_4 was investigated to design a stable and superior catalyst for CO hydrogenation into linear hydrocarbons through Fischer–Tropsch Synthesis (FTS) reaction. Enhanced structural stability was observed in ordered-mesoporous Co_3O_4 even under hydrogen-excess conditions after modification with a metal oxide pillar of Al_2O_3. The mesoporous Co_3O_4 was synthesized using a hard template of highly ordered three dimensional mesoporous KIT-6. A small number of metal oxide pillars such as Al_2O_3, Mn_2O_4, and SiO_2 with 5 wt% were subsequently added to the ordered-mesoporous Co_3O_4 through the incipient wetness impregnation method. The Al_2O_3-modifed mesoporous Co_3O_4 catalyst demonstrated superior CO conversion with a stable activity in CO hydrogenation reaction. The enhanced catalytic stability seems to be attributable to the lower mobility of the Al_2O_3 pillar which formed stronger interactions with the mesoporous Co_3O_4 inner surfaces. The Al_2O_3 modification can effectively stabilize ordered-mesoporous structures of Co_3O_4 by acting as an ordered mesoporous channel reactor and enhancing the transport rate of hydrocarbons formed during FTS reaction.

1. Introduction

The synthesis of mesoporous materials with regular nanoscale pore structures has been investigated extensively since mesoporous silica such as MCM-41 was successfully applied to reactions to overcome the mass transfer limitation of general micropore zeolites with pore sizes less than 1 nm. Since mesoporous materials have relatively large pore sizes which can be easily controlled by varying the carbon chain length of surfactants, they have been widely used in various catalytic reactions for the transformation of larger molecules or the suppression of wax deposition in the micropores of catalysts. The pore blockage from wax deposition inside of pores has been largely reported as the main reasons for the deactivation especially for Fischer–Tropsch Synthesis (FTS) reactions [1,2]. FTS reaction is known to be one of the chemical processes that convert syngas into clean liquid fuels to reduce the pollution emissions from stationary or mobile sources. Therefore, its use in syngas to liquids (GTL) technology has been largely investigated due to the possible utilization of new feedstock originating from biomass, coal, natural gas, or shale gas in recent applications, especially for further possible application in GTL-FPSO (floating, production, storage, and off-loading) using micro-channel type reactors operating at high gas velocity [2].

The cobalt-based FTS catalysts have been generally known to favorably produce higher molecular weight linear hydrocarbons through ASF (Anderson–Schulz–Flory) polymerization. Because cobalt-based FTS catalysts are not only advantageous for their selectivity to linear paraffins but also their long lifetimes with lower water–gas shift activity [2–4], they have been extensively investigated for use in designing a stable and superior catalyst with largely exposed metallic cobalt particles on the commercial supports [5–7]. Therefore, the use of highly ordered-mesoporous silica with large surface areas has been evaluated to synthesize highly dispersed cobalt particles, which are responsible for the higher metallic surface area of cobalt and resulted in higher catalytic activity and productivity [5,8–11]. The syntheses and applications of two or three dimensional ordered-mesoporous metal oxides such as Co_3O_4 [12–14] have been abundantly reported by many researchers

* Corresponding author. Fax: +82 31 290 7272.
E-mail address: finejw@skku.edu (J.W. Bae).

http://dx.doi.org/10.1016/j.apcatb.2015.06.024
0926-3373/

in the applications to various catalytic reactions such as oxidation reactions [15–20] or battery technologies [21,22] due to their intrinsic characteristics such as regular pore structures and active metal frameworks. However, ordered-mesoporous Co_3O_4 has not been sufficiently investigated till now as far as we know due to its unstable structure under hydrogen-rich condition [23], especially in CO hydrogenation reactions such as the FTS reaction.

In the present study, we focused on designing a stable ordered-mesoporous Co_3O_4 to enhance catalytic stability and activity even under hydrogen-rich environment by simply incorporating metal oxide pillars such as Al, Mn and Si oxides inside pores, since we had observed the easy collapse of unmodified mesoporous Co_3O_4 structures under the FTS reaction in our previous work [24]. The ordered mesoporous Co_3O_4 was previously synthesized using nano-replication and the selected metal oxide pillaring materials was subsequently added through simple wet impregnation. The structural stability and high catalytic activity of the modified mesoporous Co_3O_4, which can effectively operate even at a high space velocity, was mainly explained by characterizing the structural changes during the FTS reaction, the distribution and mobility of pillaring materials and the variation of cobalt surface properties on the mesoporous Co_3O_4.

2. Experimental

2.1. Synthesis of the metal oxide pillared mesoporous Co_3O_4 and activity test

Ordered-mesoporous Co_3O_4 was prepared through a hard template method using KIT-6 followed by subsequent incipient wetness impregnation of cobalt precursor. A highly ordered mesoporous KIT-6 was synthesized using a triblock copolymer, $EO_{20}PO_{70}EO_{20}$ (Pluronic P123 of poly(ethyleneoxide)-poly(propyleneoxide)-poly(ethyleneoxide), supplied by Aldrich) as a structure-directing agent through the reported typical synthetic procedures [25–27]. Briefly, P123 copolymer was dissolved in distilled water, and aqueous HCl solution (37 wt%) was mixed with an aqueous solution of well dissolved P123 copolymer under vigorous stirring at 35 °C. After mixing, *n*-butanol was added to the above solution and stirred for 1 h followed by the addition of tetraethoxysilane (TEOS, supplied by Alfa Aesar, 99.9%). After vigorous stirring at 35 °C for 24 h, the milky precipitant was hydrothermally treated in an autoclave for 24 h at 100 °C under static condition. The final solution was filtered and the white precipitant was dried at 100 °C. In order to remove the P123 surfactant, the white powder was washed with an ethanol/HCl solution, and the fine powder was subsequently calcined at 550 °C for 6 h at a heating rate of 1 °C/min to make a hard KIT-6 template.

The synthetic procedure of ordered-mesoporous Co_3O_4 using mesoporous KIT-6 as a hard templating material followed the previous report [15]. Briefly, the mesoporous KIT-6 was pretreated by heating at 100 °C for 1 h, and cobalt nitrate hexahydrate ($Co(NO_3)_2{\cdot}6H_2O$, Samchun Chem., 97.0%) precursor of 9.5 g was separately dissolved in 10 ml distilled water. The purple-colored aqueous cobalt solution was impregnated into the mesoporous KIT-6, and the homogeneously mixed gel containing the cobalt precursor with a KIT-6 template was dried at 80 °C overnight and calcined at 550 °C for 3 h at a heating rate of 1 °C/min. The as-prepared black cobalt oxide power was washed with 2 M NaOH aqueous solution to extract the mesoporous KIT-6 template, and washed with water followed by acetone for several times. Finally, the template-free ordered-mesoporous Co_3O_4 was further dried at 100 °C, and denoted as meso-Co_3O_4.

A metal oxide pillared meso-Co_3O_4 was prepared through incipient wetness impregnation method using a fixed 5 wt% Al, Mn, and Si metal precursors separately based on the weight of Co_3O_4. For preparing 5 wt% metal oxide pillared meso-Co_3O_4, 2.99 g of $Al(NO_3)_3{\cdot}9H_2O$ (Daejung Chem., 97.0% purity), 0.28 g of $Mn(NO_3)_2{\cdot}xH_2O$ (Junsei, 97.0% purity), or 1.17 g of TEOS (Alfa Aesar, 99.9% purity) precursors were separately dissolved using 2.0 ml of distilled water in a slurry of meso-Co_3O_4 to partially deposit the pillaring metal oxides into mesopores of the meso-Co_3O_4. The metal oxide pillared meso-Co_3O_4 gel was dried at 80 °C overnight, and the powder was calcined at 550 °C for 3 h at a heating rate of 1 °C/min. The as-prepared final catalysts were denoted as Al/meso-Co_3O_4, Mn/meso-Co_3O_4, and Si/meso-Co_3O_4, respectively.

Catalytic activity was measured using a fixed bed reactor with an outer diameter of 12.7 mm with 0.1 g (volume of 0.088 cm^3) of the as-prepared catalyst mixed with 0.5 g of α-Al_2O_3 diluent, which was prepared by calcining as-received Puralox γ-Al_2O_3 at 1000 °C for 5 h. Prior to the reaction, metal oxide pillared meso-Co_3O_4 was reduced under a flow of 5 vol%H_2/N_2 at 400 °C for 12 h. After reduction, the reaction was cooled to room temperature and a feed gas composed of $H_2/N_2/CO$ = 62.84/5.60/31.56 was introduced as reported in detail in our previous work [28]. The reaction pressure was increased to 2.0 MPa by using a back pressure regulator, and the temperature was increased to 230 °C at the fixed weight hourly space velocity (WHSV) of 24,000 L(mixed gas)/(kg_{cat} h) for the reaction duration of 40 h. The effluent gases from the reactor were collected and analyzed using an online gas chromatograph (YoungLin Acme 6000 GC, Korea) equipped with a GS-GASPRO capillary column connected to a flame ionization detector (FID) for analyzing the hydrocarbons formed, and a Carboxen 1000 packed column connected to a thermal conductivity detector (TCD) for analyzing H_2, CO, CO_2 and CH_4. CO conversion and product distribution on the metal oxide pillared meso-Co_3O_4 were calculated based on the carbon balance from the results of the on-line GC analyses.

2.2. Catalyst characterizations

The powder X-ray diffraction (XRD) patterns from the fleshly calcined metal oxide pillared meso-Co_3O_4 were measured using a Rigaku D/MAX-2200 V diffractometer operating at 40 kV and 40 mA with Cu-Kα radiation of 0.15406 nm with a scanning rate of 5°/min at the diffraction ranges of 2θ = 10–80°. The particle size of meso-Co_3O_4 was calculated from the value of the full width at half maximum (FWHM) by using the Debye–Scherrer equation and by selecting the most intensive diffraction peak of Co_3O_4 at 2θ = 36.8°. In addition, the particle size of metallic cobalt was also determined from the calculated Co_3O_4 particle size by using the correlation of the relative molar volume of metallic cobalt and Co_3O_4 with the equation of $d(Co^0) = 0.75 \times d(Co_3O_4)$ [2].

The surface area, pore volume and average pore diameter of the four different meso-Co_3O_4 were characterized by the Brunauer–Emmett–Teller (BET) method. Prior to N_2 sorption experiment, the catalyst was degassed under vacuum condition at 350 °C for 3 h. The nitrogen adsorption-desorption isotherms were obtained at −196 °C using a Micromeritics ASAP 2000 analyzer equipped with a vacuum pump maintained at 10^{-6} Pa. The pore size distribution of the as-prepared four different meso-Co_3O_4 were also determined by the BJH (Barrett–Joyner–Halenda) method from the desorption isotherm. Surface morphologies and the variation of particle sizes on the fresh and used metal oxide pillared meso-Co_3O_4 were characterized using transmission electron microscopy (TEM) with a TECNAI G2 instrument operated at an accelerating voltage of 200 kV.

H_2-chemisorption analysis was carried out at 100 °C under a static condition using the Micromeritics ASAP 2000 in order to measure the surface area (m^2/gCo) of metallic cobalt. Prior to chemisorption analysis, the as-prepared 0.5 g sample was reduced at 400 °C for 12 h under a flow of 5 vol%H_2/N_2. The surface area

of metallic cobalt was calculated with the H/Co stoichiometry assumed to be 1.0. The degrees of reduction of metal oxide pillared meso-Co_3O_4 were also measured by O_2 titration, and the particle size of metallic cobalt was corrected by considering the degree of reduction. The degree of reduction was calculated using the equation [amount of O_2 consumed during O_2 titration ($mmolO_2$)]/[theoretical amount of consumable O_2 after full reduction of cobalt oxides ($mmolO_2$) with the assumption of $(3Co + 2O_2 \rightarrow Co_3O_4)] \times 100$.

Temperature-programmed reduction (TPR) was carried out to verify the reducibility of Co_3O_4 particles and a different interaction between meso-Co_3O_4 and the metal oxide pillars using a BELCAT instrument equipped with TCD. Prior to TPR measurement, the meso-Co_3O_4 were flushed under flowing Ar at 350 °C for 2 h in a quartz tube reactor to remove adsorbed water and impurities, and this was followed by cooling to 50 °C. The reducing gas of 5 vol%H_2/Ar was introduced to the reduced sample at a flow rate of 30 ml/min in the temperature ranges of 50–1000 °C at a heating rate of 10 °C/min. The effluent gases were passed through a molecular sieve to remove the water formed, and the reduction patterns of metal oxide pillared meso-Co_3O_4 were obtained.

The electronic state and binding energy (BE) of $Co2p_{3/2}$, Al2p, $Mn2p_{3/2}$, and Si2p on the fresh catalyst were analyzed using X-ray photoelectron spectroscopy (XPS; ESCALAB MK-II) analysis. During the XPS experiment, Al Kα monochromatized line (1486.6 eV) was used, and the vacuum level was kept at around 10^{-7} Pa. The measured BEs were corrected with a reference BE of C1s (284.6 eV). In addition, the intensity ratios of I_M/I_{Co}, defined as the integrated area of each metal (Al, Mn, or Si) divided by that of cobalt which was corrected by using atomic sensitivity factor of metals, were calculated to elucidate the variation of surface concentration before and after the FTS reaction. The integrated areas of metals were previously corrected using atomic sensitivity factors [29], and the intensity ratios of I_M/I_{Co} were calculated using the equation of I_M/I_{Co} = (area of metal/area of Co) × (S_M/S_{Co}), where atomic sensitivity factor (S) of S_{Co} = 4.5, S_{Al} = 0.11, S_{Mn} = 2.1, and S_{Si} = 0.17.

Fourier transform infrared (FT-IR) spectra on the used metal oxide pillared mseo-Co_3O_4 were obtained using PerkinElmer Spectrum 2000 spectrometer which has a spectral resolution of 2 cm^{-1} to confirm the types of hydrocarbons formed during the FTS reaction.

Thermogravimetric analysis (TGA) on the used metal oxide pillared meso-Co_3O_4 (after reaction of 40 h) was carried out using a DMA instrument. The used catalyst (30 mg) just after drying at 100 °C for 2 h in an oven was heated from 50 to 900 °C at a rate of 10 °C/min under an air flow of 30 ml/min.

3. Results and discussion

3.1. Physicochemical properties of metal oxide pillared meso-Co_3O_4 catalysts

XRD patterns of the fresh metal oxide pillared meso-Co_3O_4 are displayed in Fig. 1. The characteristic diffraction peaks of Co_3O_4 were clearly observed at 2θ = 19.0, 31.2, 38.5, 44.8, 59.3 and 65.2°, which correspond to the spinel crystal planes Co_3O_4 assigned to (1 1 1), (2 2 0), (3 1 1), (4 0 0), (5 1 1) and (4 4 0) [30]. These characteristic diffraction peaks of Co_3O_4 can also include the crystal phases of $CoAl_2O_4$, which has almost identical diffraction peaks as Co_3O_4 structures [31,32] but minimal formation at our pretreatment condition. The average cobalt particle sizes in the fresh catalysts were calculated using the Debye–Scherrer equation by taking into account the most intense diffraction peak at 2θ = 36.8° corresponding to the (3 1 1) crystal plane of Co_3O_4. The calculated particle sizes of Co_3O_4 were found to be 14.8, 16.9, 14.5 and 14.5 nm on the meso-Co_3O_4, Al/meso-Co_3O_4, Mn/meso-Co_3O_4, and Si/meso-Co_3O_4, respectively, as summarized in Table 1. These particle size variations of cobalt were not significant according to the types of metal oxide pillars, and seemed to be attributable to the similar grain size of the main framework of meso-Co_3O_4 even after modification with metal oxide pillars. However, somewhat larger Co_3O_4 particle sizes were observed on the Al/meso-Co_3O_4 due to the possible formation of strongly interacted meso-Co_3O_4 framework particles with non-reducible Al_2O_3. In addition, the particle size of metallic cobalt was also calculated from that of Co_3O_4 by using the correlation of a relative molar volume of Co_3O_4 with metallic Co through $d(Co^0) = 0.75 \times d(Co_3O_4)$ [33]. Since the particle sizes of metallic cobalt over 6 nm are known to be little effects on the intrinsic catalytic activity changes due to structural insensitive natures of larger cobalt particles for FTS reaction [2], the calculated particle sizes of metallic cobalt were found to be enough larger sizes above 10 nm on all tested catalysts.

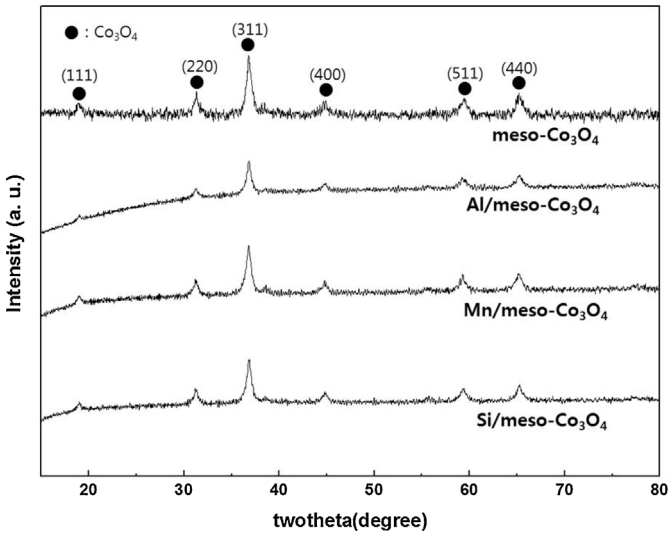

Fig. 1. XRD patterns of the fresh metal oxide pillared meso-Co_3O_4 catalysts.

The surface area, pore volume and average pore diameter of the as-prepared catalysts are presented in Table 1. BET surface area and pore volume showed a tendency to decrease in the order of meso-Co_3O_4 > Al/meso-Co_3O_4 > Mn/meso-Co_3O_4 > Si/meso-Co_3O_4 with the values of 104, 98, 71, and 41 m^2/g_{cat}, respectively, while the average pore diameters showed an inverse trend by representing the values of 5.0–10.8 nm with the larger pore diameters on Si/meso-Co_3O_4. This suggests that Al pillaring material was well dispersed on the inner surfaces of meso-Co_3O_4 compared to the other metal oxide pillars. In addition, the stronger interaction of well-dispersed Al_2O_3 pillar on the meso-Co_3O_4 surfaces may be responsible for the observed higher surface area and larger pore volume on the Al/meso-Co_3O_4. As shown in Fig. 2, N_2 adsorption-desorption curves show a characteristic type IV isotherm, and the hysteresis suggests that the ordered mesopores on all as-prepared catalysts were successfully synthesized even after the metal oxide pillaring step. The larger pore diameter observed on the Mn/meso-Co_3O_4 and Si/meso-Co_3O_4 seems to be due to the pore blockage on the outer surfaces of meso-Co_3O_4 by possibly forming interparticular mesopores through a partial structural collapse [34]. The relatively weak interactions between meso-Co_3O_4 and metal oxide pillars with a partial blockage of mesopores through an uneven distribution could be mainly responsible for the lower surface area of Mn/meso-Co_3O_4 and Si/meso-Co_3O_4.

Table 1
Physicochemical properties of the metal oxide modified ordered-mesoporous Co_3O_4.

Catalysts	XRD		BET (fresh/reduced)			H_2-chem.	O_2 titration	CO-IR
	Crystallite size of Co_3O_4 (nm)	Crystallite size of Co[a](nm)	Surface area (m^2/g)	Pore volume (cm^3/g)	Pore diameter (nm)	Surface area of cobalt (m^2/g Co)	Degree of reduction (%)	Ratios of CO adsorption on Co^{n+}/Co^0
meso-Co_3O_4	14.8	11.1	104/53	0.19/0.18	5.0/15.3	8.1	63.1	2.32
Al/meso-Co_3O_4	16.9	12.7	98/72	0.21/0.13	8.1/7.3	31.0	40.3	1.12
Mn/meso-Co_3O_4	14.5	10.9	71/41	0.19/0.11	8.8/11.4	10.7	44.2	1.49
Si/meso-Co_3O_4	14.5	10.9	41/33	0.12/0.09	10.8/12.7	14.8	23.1	3.29

[a] The particle size of metallic cobalt was obtained from the Co_3O_4 particle size by using the correlation for a relative molar volume of metallic cobalt with the equation $d(Co^0) = 0.75 \times d(Co_3O_4)$.

3.2. Surface area of metallic cobalt and reducibility of Co_3O_4

The surface area of the metallic cobalt on the metal oxide pillared meso-Co_3O_4 was measured by H_2 chemisorption, and the results are summarized in Table 1. Even though the particle sizes of Co_3O_4 on the as-prepared catalysts were found to be similar at around 15 nm (from XRD analysis), albeit with significantly different surface areas of 41–104 m^2/g_{cat}, the surface area of metallic cobalt has no clear correlation with this observation. A larger metallic cobalt surface area was observed on the Al/meso-Co_3O_4 with a value of 31.0 m^2/g_{Co}, while a smaller surface area was observed on the meso-Co_3O_4 with the value of 8.1 m^2/g_{Co}. However, the moderate metallic cobalt surface areas were observed on the Mn/meso-Co_3O_4 and Si/meso-Co_3O_4 with values of 10.7 and 14.8 m^2/g_{Co}, respectively. These differences in surface areas measured by BET and H_2 chemisorption were mainly attributed to the partial meso-structural collapse during reduction treatment at 400 °C, especially on the meso-Co_3O_4 as previously reported in our previous work [24]. It may also be due to the pore blockage by pillaring materials such as Mn and Si metal oxides. However, the higher surface area of metallic cobalt observed on Al/meso-Co_3O_4 suggests the presence of stable meso-structures with a higher dispersion of Al pillars after modification with the Al species inside the meso-Co_3O_4 pores. In addition, the degree of reduction measured by O_2 titration was found to be in the range of 23.1–63.1% and the reduction was found to be in the order of meso-Co_3O_4 > Al/meso-Co_3O_4 ≈ Mn/meso-Co_3O_4 > Si/meso-Co_3O_4. Generally, the transition metal oxides having a lower melting point and smaller particle size have been known to be responsible for showing the characteristics of a higher mobility on the catalysts surfaces at the much lower meting points of metal oxides [35,36]. Based on the these general observations on metal oxides, all pillaring metal oxides on the meso-Co_3O_4, especially for the Al_2O_3, are well dispersed on the inside of mesoporous Co_3O_4 surfaces which was also confirmed through the variations of surface areas after modification. However, manganese oxide and silica pillars intrinsically possessed relatively lower melting points compared to the Al_2O_3 species on the pores of meso-Co_3O_4. Therefore, the manganese oxides and silica pillars could more easily cover the surfaces of the active metallic cobalt by a facile migration during the reduction and FTS reactions. The H_2-reduction trends and surface area variations after modification with pillaring metal oxides seem to be attributed to the possible local encapsulation of cobalt particles within the oxidized Si and Mn species due to their facile mobility resulting from the lower melting temperatures of these metals compared with Al_2O_3 species [35,36]. Therefore, the higher

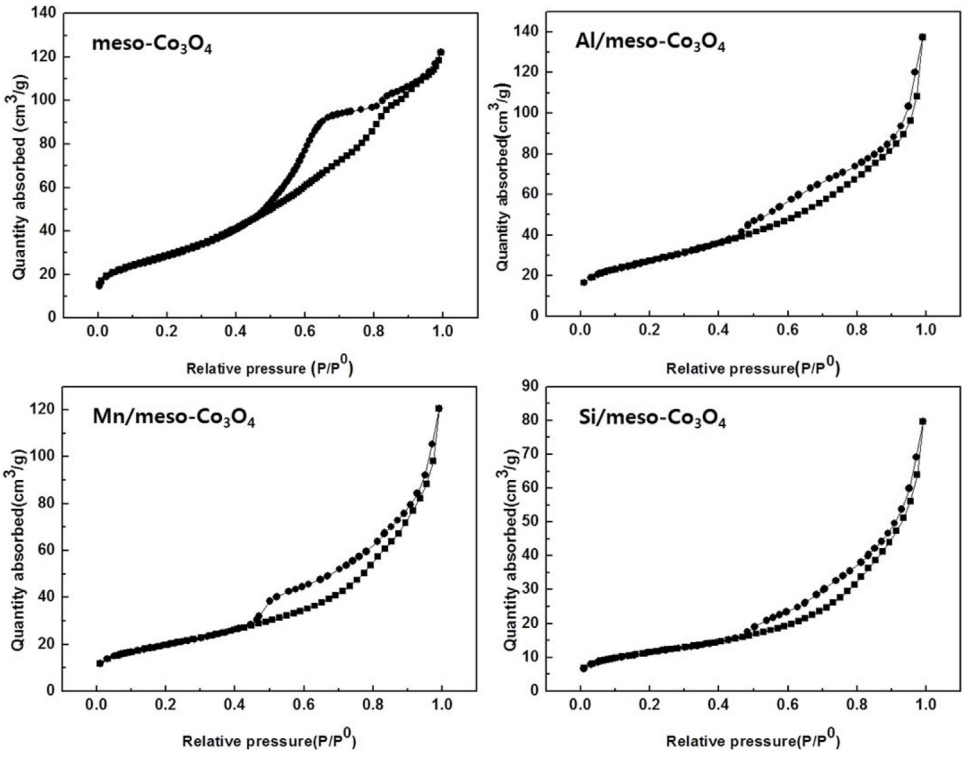

Fig. 2. N_2 adsorption–desorption isotherms on the fresh metal oxide pillared meso-Co_3O_4 catalysts.

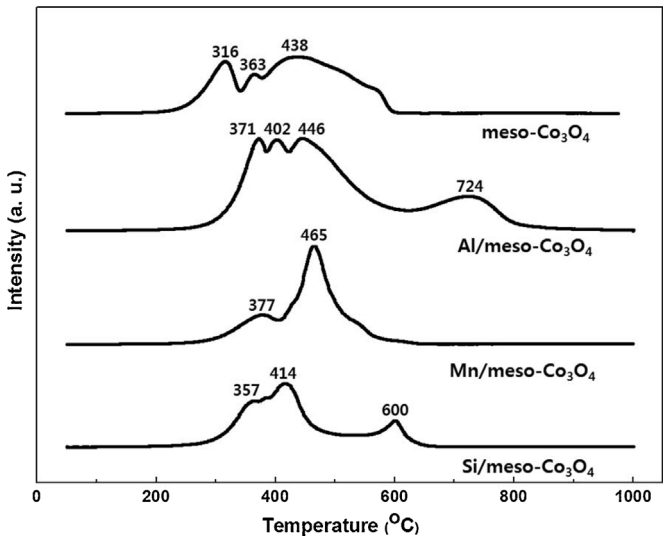

Fig. 3. TPR profiles of the fresh metal oxide pillared meso-Co_3O_4 catalysts.

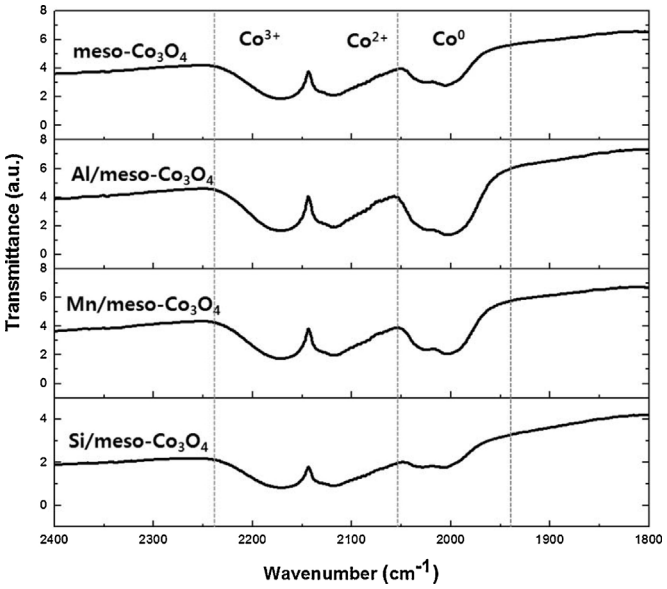

Fig. 4. FT-IR spectra of the adsorbed CO molecules on the metal oxide pillared meso-Co_3O_4 catalysts.

surface area of metallic cobalt on the Al/meso-Co_3O_4 suggests stronger interactions between meso-Co_3O_4 surfaces and thermally stable Al_2O_3 particles even under the reduction and FTS reaction conditions. It may also be responsible for the stable formation of mesopore structures, resulting in a higher catalytic activity and stability on the Al/meso-Co_3O_4 compared to other meso-Co_3O_4, Mn/meso-Co_3O_4, Si/meso-Co_3O_4.

The reduction behaviors of the modified meso-Co_3O_4 and the interaction of cobalt particles with pillaring materials were further characterized by H_2-TPR experiment as shown in Fig. 3. The reduction patterns of Co_3O_4 particles have been generally known to proceed in two-stage reductions as follows: spinel structure $Co_3O_4 \rightarrow CoO \rightarrow$ metallic cobalt (Co^0) [4,37,38]. On the metal oxide pillared meso-Co_3O_4, the first characteristic reduction peak below 400 °C can be assigned to the reduction of Co_3O_4 to CoO, and the second peak below 600 °C to the reduction of CoO to metallic cobalt [4,24]. On the meso-Co_3O_4, the maximum reduction peaks were observed at 316 and 438 °C, in accordance with the typical two step reduction behavior of Co_3O_4, and a shoulder peak was observed at 363 °C possibly due to the presence of aggregated cobalt particles during a synthesis step of meso-Co_3O_4 [24]. On the Mn/meso-Co_3O_4 and Si/meso-Co_3O_4, two distinctive reduction peaks were also observed at different temperatures of 357 and 414 °C on the Si/meso-Co_3O_4 and they shifted to higher temperature regions of 377 and 465 °C on the Mn/meso-Co_3O_4. Interestingly, the third reduction peak at around 600 °C was observed on Si/meso-Co_3O_4, and it can be attributed to the strong interaction between Co_3O_4 and SiO_2 species, possibly from forming an inactive cobalt silicate [2] or producing locally encapsulated Co_3O_4 particles with SiO_2 [35]. It also suggests the partial collapse of the mesopore structures or non-uniform distribution of pillaring materials on the meso-Co_3O_4 [39–41]. Interestingly, reduction peaks with different characteristic were observed on the Al/meso-Co_3O_4 at the temperatures of 371, 402, 446, and 724 °C, and they were shifted to much higher temperatures compared to the meso-Co_3O_4. Even though the characteristic peaks below 500 °C on the Al/meso-Co_3O_4 appeared at somewhat higher temperature regions due to newly formed strong cobalt–alumina interactions similar to those on the meso-Co_3O_4, the higher reduction peak observed at around 724 °C seems to be mainly due to the formation of spinel cobalt aluminate [2]. Although catalytic activity can be decreased by the strong interaction of the meso-Co_3O_4 with non-reducible metal oxides such as Al_2O_3 and SiO_2 through the formation of the inactive spinel structures [2], the extent of encapsulation by pillaring materials and the structural stability of meso-Co_3O_4 seems to be more important for obtaining catalytic stability even under H_2-rich reductive environments as confirmed by XPS and TEM analysis in the following section.

To further verify the reducibility of metal-oxide pillared meso-Co_3O_4, the peak patterns of the FT-IR analysis for the adsorbed CO molecules on the reduced catalysts were displayed in Fig. 4 to further support the oxidation states of cobalt particles and different product distribution. The adsorption peaks in the wavenumber ranges of 2050–2070 cm^{-1} and 1990–2030 cm^{-1} have been known to be attributed to the characteristic ones for the adsorbed CO molecules on the metallic cobalt species [2]. In addition, the characteristic peaks with the wavenumbers of 2150–2160 cm^{-1} and 2180–2200 cm^{-1} are also known to represent the adsorbed CO molecules on the Co^{2+} or Co^{3+} species, respectively [2]. The intensity ratios of the adsorbed CO molecules on the partially oxidized cobalt (Co^{2+} and Co^{3+}) to the adsorbed CO molecules on the metallic cobalt are summarized in Table 1. The intensity ratios of the values around 1.12–3.29 are increased in the order of Al/meso-Co_3O_4 < Mn/meso-Co_3O_4 < meso-Co_3O_4 < Si/meso-Co_3O_4 which suggest that the higher CO hydrogenation activity on Al/meso-Co_3O_4 and vice versa on Si/meso-Co_3O_4 by forming a non-reducible cobalt oxides largely. In addition, the observed lower ratio on the meso-Co_3O_4, which was found to be highly reduced among four catalysts, seems to be attributed to the structural collapses of meso-Co_3O_4 by suppressing the amounts of the exposed metallic cobalt species. Therefore, a high reduction property with a stable mesopore structure on the Al/meso-Co_3O_4 may be mainly responsible for an enhanced activity and stability through the Al_2O_3 modification of the inner pores of meso-Co_3O_4.

3.3. *Stability of mesoporous Co_3O_4 structures after pillar addition*

To further verify the formation of mesoporous structures on the fresh metal oxide pillared meso-Co_3O_4, TEM analyses were carried out and the images are displayed in Fig. 5. The ordered regular pores with a diameter of around 6–8 nm were clearly visible, and the mesoporous structures remained even after the metal oxide pillaring step. However, somewhat larger pore diameters of around 8 nm were observed on the Al/meso-Co_3O_4, Mn/meso-

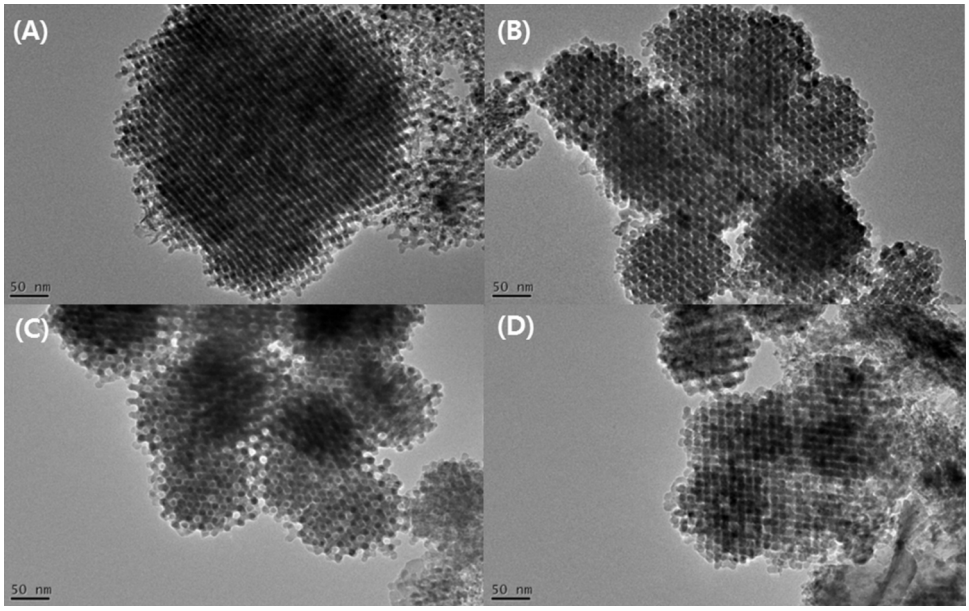

Fig. 5. TEM images of the fresh (A) meso-Co_3O_4 (B) Al/meso-Co_3O_4 (C) Mn/meso-Co_3O_4 and (D) Si/meso-Co_3O_4 catalyst.

Co_3O_4, and Si/meso-Co_3O_4 compared to the meso-Co_3O_4 with an average diameter of around 6 nm. This observation suggests the possible insertion of a bulk metal oxide pillar to the inside surfaces of the Co_3O_4 mesopores. In addition, some local irregular and crushed structures were observed on the Mn/meso-Co_3O_4 and Si/meso-Co_3O_4 compared to the Al/meso-Co_3O_4 which can greatly affect the catalytic stability. The Al_2O_3 pillaring material seemed to be well dispersed inside the meso-Co_3O_4 without significant structural collapse even after the pillaring step. Al_2O_3 can act as a structure stabilizer under the reductive environments by strongly interacting with the meso-Co_3O_4 surfaces as confirmed by H_2-TPR analysis. The much larger particle sizes of Co_3O_4 shown in the TEM images were not well matched with the results of XRD analysis due to the following possible reasons; (1) the oxygen titration method used for calculating the particle size of Co_3O_4 can underestimate the degree of reduction due to simultaneous formation of the CoO phase, which is more stable than Co_3O_4 below 400 °C [42–44], (2) Even though the particle sizes of Co_3O_4 calculated from XRD are generally well matched with the metallic size of cobalt particles analyzed by chemisorption, the particle size difference between Co_3O_4 and metallic Co generally increase with the increase of the pore diameter of the support as a result of large cobalt oxide particles breaking into smaller particles during the drying or reduction step [45]. These may be the reasons for the frequent observation that the particle sizes of Co_3O_4 inside pores are larger than the pore diameter of the support [46]. However, the stability of mesoporous structures and the particle size variation during catalyst preparation can be fully explained using the above mentioned techniques.

In addition, the structural stabilities of the metal oxide pillared meso-Co_3O_4 under reductive conditions were further confirmed through TEM and N_2 sorption analyses by characterizing the reduced catalysts after H_2 treatment at 400 °C for 12 h. Supplementary Figs. S1 and S2 represented the N_2 adsorption–desorption isotherms and the pore size distributions on the reduced metal oxide pillared meso-Co_3O_4 catalysts. Compared with the Fig. 2, N_2 adsorption–desorption curves showed a characteristic type IV isotherm with the suppressed extent of hysteresis, which reveals the partial collapse of ordered mesopore structures during the reduction step, especially on the meso-Co_3O_4 and Mn/meso-Co_3O_4 as confirmed by the pore size distribution in Supplementary Fig. S2. As summarized in Table 1, the surface areas after reduction were significantly decreased in the range of 33–72 m^2/g, however, Al/meso-Co_3O_4 still showed a higher surface area of 72 m^2/g and vice versa on the Al/meso-Co_3O_4 with the value of 33 m^2/g. The pore volume on the reduced catalysts was also decreased by showing the similar trend of the surface area. The average pore diameters are found to be 7.3–15.3 nm and they were significantly increased on all mesoporous catalysts except for the Al/meso-Co_3O_4 (8.1 nm on the calcined catalyst and 7.3 nm on the reduced one) which suggest the enhanced stability of mesopore structures. In addition, the Supplementary Fig. S3 further represented the TEM images of the reduced metal oxide pillared meso-Co_3O_4, which also confirms that the ordered mesoporous structures are locally collapsed on all catalysts. However, the extents of these collapses are not significant on Al/meso-Co_3O_4 due to the thermally stable Al_2O_3 pillar formation. From these results, we can suggest that the partial collapses of mesoporous structures seem to happen possibly from the reduction step, which could be further collapsed severely during the FTS reaction, except for the Al_2O_3 pillared meso-Co_3O_4 due to the strong interaction with Al_2O_3 pillar formed on the surfaces of meso-Co_3O_4. Therefore, the ordered mesoporous structures on the Al/meso-Co_3O_4 are robust against structural collapses even after the FTS reaction, which were supported by the suppressed aggregation of Co_3O_4 particles with a structural stability of the Al/meso-Co_3O_4 compared with the meso-Co_3O_4 and Mn/meso-Co_3O_4.

3.4. Catalytic activity and stability according to the types of metal oxide pillars

Catalytic activities such as CO conversions, reaction rates and turn-over frequencies (TOF) on the metal oxide pillared meso-Co_3O_4, which are defined as the reacted CO μmol/(g_{cat} s) and the reacted CO molecules/(surface cobalt atom s), respectively, are summarized in Table 2. The CO conversions were found to be 23.0, 85.6, 1.1 and 3.0 mol% on the meso-Co_3O_4, Al/meso-Co_3O_4, Mn/meso-Co_3O_4, and Si/meso-Co_3O_4, respectively, with the highest CO conversion on the Al/meso-Co_3O_4, even at a higher space velocity of 24,000 L/(kg_{cat} h). No catalytic activity on the α-Al_2O_3 diluent itself, which was prepared by calcining as-received Puralox γ-Al_2O_3 at 1000 °C for 5 h, was observed with time on stream as shown in Supplementary Fig. S4 by confirming that the FTS activities were uniquely attributed to the active sites on

Table 2
Catalytic performances on the metal oxide pillared meso-Co_3O_4 catalysts.

Catalysts	Activity[a]			Product distribution (C-mol%)	
	CO conv. (C-mol%)	Rate[b]	TOF[b]	$C_1/C_2–C_4/C_5+$	Olefins in $C_2–C_4$ (%)
meso-Co_3O_4	23.0	20.0	0.134	8.7/15.3/76.0	20.4
Al/meso-Co_3O_4	85.6	80.0	0.148	11.5/11.1/77.4	11.2
Mn/meso-Co_3O_4	1.1	1.0	0.006	3.3/9.7/87.0	59.6
Si/meso-Co_3O_4	3.0	2.7	0.004	7.4/12.1/80.5	60.6

[a] FTS reaction was carried out at the following reaction conditions; $T = 230\,^{\circ}C$, $P = 2.0$ MPa, WHSV = 24,000 L/(kg_{cat} h), and feed gas composition of $H_2/N_2/CO = 62.84/5.60/31.56$.
[b] The rate was defined as reacted CO μmol/(g_{cat} s), and TOF as reacted CO molecules/(surface cobalt atom s).

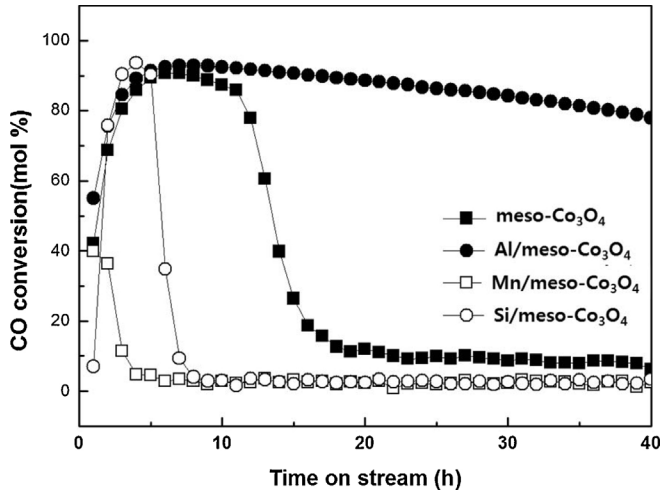

Fig. 6. Catalytic activity on the metal oxide pillared meso-Co_3O_4 catalysts with time on stream (h).

the mesoporous Co_3O_4. As shown in Fig. 6, the stability of the metal oxide pillared meso-Co_3O_4 was apparent, and the most stable catalytic activity was observed on the Al/meso-Co_3O_4. The calculated reaction rate and TOF were also found to be higher on the Al/meso-Co_3O_4 with values of 80 [reacted CO μmol/(g_{ca} s)] and 0.148 [reacted CO molecules/(surface cobalt atom s)], respectively. However, significantly lower catalytic activity was observed on the Mn/meso-Co_3O_4 and the Si/meso-Co_3O_4 with TOF values of 0.006 and 0.004 molecules/(surface cobalt atom s) compared to that of the meso-Co_3O_4 with a value of 0.134 molecules/(surface cobalt atom s). In general, the site-time yields of CO on cobalt-based catalysts, defined as the converted CO molecules/(surface CO atom s) [6], were reported in the range of $1.6 \times 10^{-2} - 3.0 \times 10^{-2}$ [s^{-1}], and the present results showed a somewhat larger values due to the enhanced mass transport of products and the stability of meso tructures in the Al/meso-Co_3O_4. The lower catalytic activity on the Mn/meso-Co_3O_4 and the Si/meso-Co_3O_4 seems to be due to the lower metallic surface area and the lower degree of reduction. The Al and Mn pillared meso-Co_3O_4 showed significantly different activity in spite of their similar degrees of reduction, which can be possible attributed to the differences of active cobalt metallic sites through the different extents of structural collapses during the FTS reaction. However, the significantly lower catalytic activity on those catalysts by an order of magnitude as compared to that of the meso-Co_3O_4 cannot be simply explained by the differences in higher metal surface areas of around 10.7–14.8 m^2/g_{Co} compared to 8.1 m^2/g_{Co} on the meso-Co_3O_4. Therefore, the different catalytic activities were also explained by using the encapsulation phenomena of the collapsed cobalt particles with Mn or Si pillaring materials by simultaneous suppression of syngas transport.

In terms of product distributions on the metal oxide pillared meso-Co_3O_4, a slightly higher selectivity to light hydrocarbons was observed on the most active Al/meso-Co_3O_4 compared to the meso-Co_3O_4. The CH_4 selectivity was found to decrease in the order of Al/meso-Co_3O_4 > meso-Co_3O_4 > Si/meso-Co_3O_4 > Mn/meso-Co_3O_4, all in the range of 3.3–11.5 mol%. The C_5+ selectivity was found to be inversely proportional to the CH_4 selectivity as summarized in Table 2. In general, cobalt particle sizes above 6 nm are well known to have little impact on the intrinsic catalytic activity and product distribution [2,6,39]. However, the different catalytic performances on the metal oxide pillared meso-Co_3O_4 with particle sizes around 10.9–12.7 nm seems to be due to other characteristics such as the reducibility of cobalt oxides, coke deposition, different interaction and structural stability with a possible encapsulation of metallic cobalt particles and so on. The smaller Co_3O_4 particles below a size of 6 nm are generally known to occupy a large portion of lower-coordinated surface sites, and are responsible for a lower intrinsic activity and higher CH_4 selectivity [39]. This can be attributed to the strong adsorption character of CO molecules which subsequently block edge or corner sites rather than to H_2-assisted dissociative adsorption of CO molecules on the larger cobalt particles [48]. It can also be attributed to the strong interaction of the metal-pillaring metal oxides, which can induce a higher oxidation state of cobalt particles by suppressing the absorption of H_2 and inevitably causes increasing CH_4 selectivity through a fast reaction rate for light hydrocarbon formation compared to the formation of the wax-like higher molecular weight linear hydrocarbons [2,47–50]. Therefore, the observed higher CH_4 selectivity on the Al/meso-Co_3O_4 seems to be mainly due to the presence of strongly interacted mainframe Co_3O_4 surfaces with Al_2O_3 pillaring particles as previously confirmed by TPR experiment. In addition, the enhanced olefin selectivity on the Si/meso-Co_3O_4 and Mn/meso-Co_3O_4 can be possibly attributed to an intrinsically lower catalytic activity and the possible promotional effect of Mn which decreases CH_4 selectivity with a concomitant increase of $C_2–C_4$ olefin and C_5+ selectivity due to the decreased availability of adsorbed H_2 on the catalyst surfaces [51–53]. The different catalytic activity and stability with a largely different product distribution were further investigated by characterizing the structural stability and the extent of surface distribution of the pillared metal oxides on meso-Co_3O_4. The possible structural collapse and partial encapsulation of the cobalt species with the metal oxide pillars were examined with the help of XPS and TEM analysis on the used metal oxide pillared meso-Co_3O_4 in the following section.

3.5. *Stability of the ordered mesoporous Co_3O_4 under reductive FTS conditions*

To further verify the observed superior activity and stability of the Al/meso-Co_3O_4, the used FTS catalysts were characterized using TEM, XPS and FT-IR analyses to confirm the roles of the deposited carbon types and the mobility of pillaring materials to the catalytic activity.

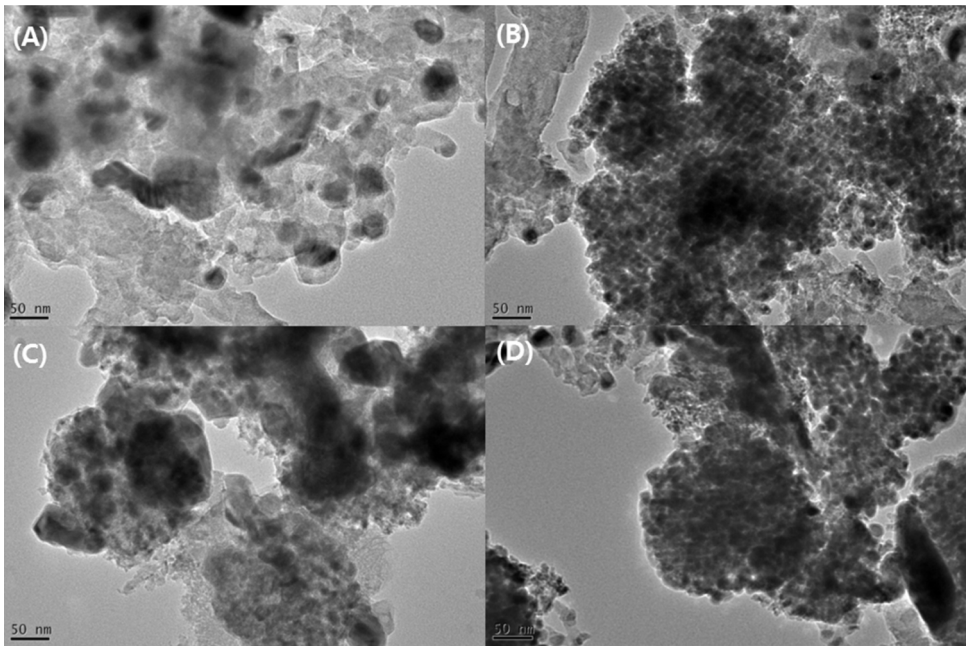

Fig. 7. TEM images of the used (A) meso-Co_3O_4 (B) Al/meso-Co_3O_4 (C) Mn/meso-Co_3O_4 and (D) Si/meso-Co_3O_4 catalyst.

TEM images of the morphologies of the used metal oxide pillared meso-Co_3O_4 after FTS reaction for 40 h are displayed in Fig. 7. Even though significant structural collapse was observed in the meso-Co_3O_4 due to the formation of larger particles above 20 nm in size, the mesoporous structures with sizes of around 8 nm on the Al/meso-Co_3O_4 clearly persisted even after the 40 h reaction and showed some local cobalt aggregates. Even though the structural stability of the Mn/meso-Co_3O_4 and Si/meso-Co_3O_4 was enhanced compared to the meso-Co_3O_4, the formation of stable mesoporous structures on the Al/meso-Co_3O_4 was found to be significant. This suggests that the structural stability can be largely enhanced on the Al/meso-Co_3O_4 due to the dispersion of Al_2O_3 pillars inside the mesopores of meso-Co_3O_4, which can be mainly responsible for higher catalytic activity and stability.

XPS spectra of $Co2p_{3/2}$ on the fresh and used metal oxide pillared meso-Co_3O_4 are displayed in Fig. 8. The BEs on the fresh catalysts as summarized in Table 3 were not significantly altered by the characteristic BEs of Co_3O_4 in the range of 780.2–780.9 eV irrespective of the types of pillaring metal oxides used. Since the small amount of pillaring metal oxides and the possible superposition of several peaks related to spinel cobalt mixed oxides such as $CoAl_2O_4$ and CoO with Co^0 peak in the BE of 780.0 eV [54,55], there was no noticeable changes of the variation of $Co2p_{3/2}$ peak. However, this observation also suggests a small amount of solid solution formation such as spinel-type cobalt aluminate or cobalt silicate [40,41,56]. Even though the BEs of $Co2p_{3/2}$ after the reaction were found to be 780.0 and 780.3 eV on the meso-Co_3O_4 and the Al/meso-Co_3O_4, suggesting the presence of partially reduced Co_3O_4 particles, BEs of $Co2p_{3/2}$ after reaction on the Mn/meso-Co_3O_4 and the Si/meso-Co_3O_4 showed significantly different values such as 781.3 and 779.8 eV, which implies the partial formation of solid solutions such as $Mn_xCo_{3-x}O_4$ and cobalt silicates. However, the observed BEs of the pillaring materials such as Al, Mn and Si metal oxides are well matched with the intrinsic characteristic BEs of Al_2O_3, MnO_2 and SiO_2 at around 75, 76, and 642, and 103 eV even after FTS reaction. Therefore, the pillaring materials can be maintained in a stable metal oxide form before and after FTS reaction. However, some strongly interacted solid solution can be partially formed on the outer surfaces of the Mn/meso-Co_3O_4 and the Si/meso-Co_3O_4, but this phenomenon was not significant on the Al/meso-Co_3O_4. On the Mn/meso-Co_3O_4, Mn cations can be easily transformed into mixed spinel compounds such as $Mn_xCo_{3-x}O_4$ by reactions with the surface-exposed meso-Co_3O_4 during the thermal treatment, and they are further transformed into MnO species under the reductive conditions [57]. It has been also reported that Mn species have a higher affinity with oxide forms than metallic forms. Therefore, the reduced metallic cobalt particles can split away from the manganese oxide particles, which will eventually lead to a rapid agglomeration of metallic cobalt and a facile structural collapse of the meso-Co_3O_4. On the Si/meso-Co_3O_4, separated mobile SiO_2 particles can form easily on the outer surfaces of the meso-Co_3O_4 during the FTS reaction due to the higher mobility of SiO_2 [46]. The thermally stable Al_2O_3 particles in an oxide form on the Al/meso-Co_3O_4 may be responsible for the enhanced stability of mesopore structures compared to other catalysts, and it was further confirmed by TEM images as shown in Fig. 7. However, a cubic $CoAl_2O_4$ spinel structure, which has the same diffraction angles as the Co_3O_4 spinel structure [31], can also form on the Al/meso-Co_3O_4 as confirmed by TPR experiments which showed a higher reduction peak at around 724 °C. This non-reducible inactive cobalt aluminate of $CoAl_2O_4$ seems to exist at the vicinity of the mesoporous metallic cobalt surfaces and its presence can enhance the structural stability of the Al/meso-Co_3O_4. The formation of less mobile and inactive Al_2O_3 (or $CoAl_2O_4$) seems to be mainly responsible for a higher dispersion of Al_2O_3 and less collapses of the mesopores in the Al/meso-Co_3O_4.

This hypothesis is further supported by the results of XPS analysis comparing the intensity ratios of pillaring metal oxides and cobalt species (defined as the integrated area ratio of I_M/I_{Co}, where M is for the intensity of the metal oxide pillars such as Al, Mn, and Si after corrections using atomic sensitivity factors [29]) as summarized in Table 3. The I_M/I_{Co} ratios were found to be 0.0013, 0.0274, and 0.0033 on the fresh Al/meso-Co_3O_4, Mn/meso-Co_3O_4, and Si/meso-Co_3O_4, respectively, by showing smaller value on the Al/meso-Co_3O_4 and larger value on the Mn/meso-Co_3O_4. This observation suggests the homogeneous distribution of the pillaring metal oxides inside the meso-Co_3O_4 pores before the reaction especially in the Al/meso-Co_3O_4. However, the I_M/I_{Co} ratios

Table 3
The summarized XPS results of the metal oxide pillared meso-Co_3O_4 catalysts.

Catalysts	XPS analysis of $Co2p_{3/2}$ and M2p				FT-IR on the used catalyst[b]
	BE (eV) of $Co2p_{3/2}$	BE (eV) of M2p	I_M/I_{Co}[a]		
	Fresh/used	Fresh/used	Before	After	I_{2920}/I_{2850}
meso-Co_3O_4	780.2/780.0	-/-	–	–	1.09
Al/meso-Co_3O_4	780.5/780.3	75.8/75.0	0.0013	0.0011	1.30
Mn/meso-Co_3O_4	780.9/781.3	642.1/642.4	0.0274	0.1519	1.15
Si/meso-Co_3O_4	780.6/779.8	103.0/103.1	0.0033	0.0086	1.19

[a] The integrated areas of metals were previously corrected using atomic sensitivity factors [29], and the intensity ratios of I_M/I_{Co} were calculated using the equation of I_M/I_{Co} = (area of metal/area of Co) × (S_M/S_{Co}), where atomic sensitivity factor (S) of S_{Co} = 4.5, S_{Al} = 0.11, S_{Mn} = 2.1, and S_{Si} = 0.17.
[b] The ratio of I_{2920}/I_{2850} represents the integrated area ratio of the peak at 2920 cm^{-1} (denoted as I_{2920}) and 2850 cm^{-1} (assigned to I_{2850}).

after FTS reaction clearly revealed significant changes according to the types of metal oxide pillars, which were found to be 0.0011, 0.1519, and 0.086 on the used Al/meso-Co_3O_4, Mn/meso-Co_3O_4, and Si/meso-Co_3O_4, respectively. The larger values of I_M/I_{Co} on the Mn/meso-Co_3O_4 and Si/meso-Co_3O_4 compared to that on the Al/meso-Co_3O_4 after FTS reaction suggest that the collapsed cobalt particles can be partially encapsulated [35,45] with the Mn or Si oxides by dominantly distributing on the outer surfaces of meso-Co_3O_4, and by suppressing the transport of syngas to the active sites resulted in showing lower catalytic activities. Based on the observed values of I_M/I_{Co}, we suggest that a lot of the impregnated Al_2O_3 in the Al/meso-Co_3O_4 may be incorporated to the framework of meso-Co_3O_4, which is responsible for a highly enhanced stability of mesopore structures with a stable catalytic activity.

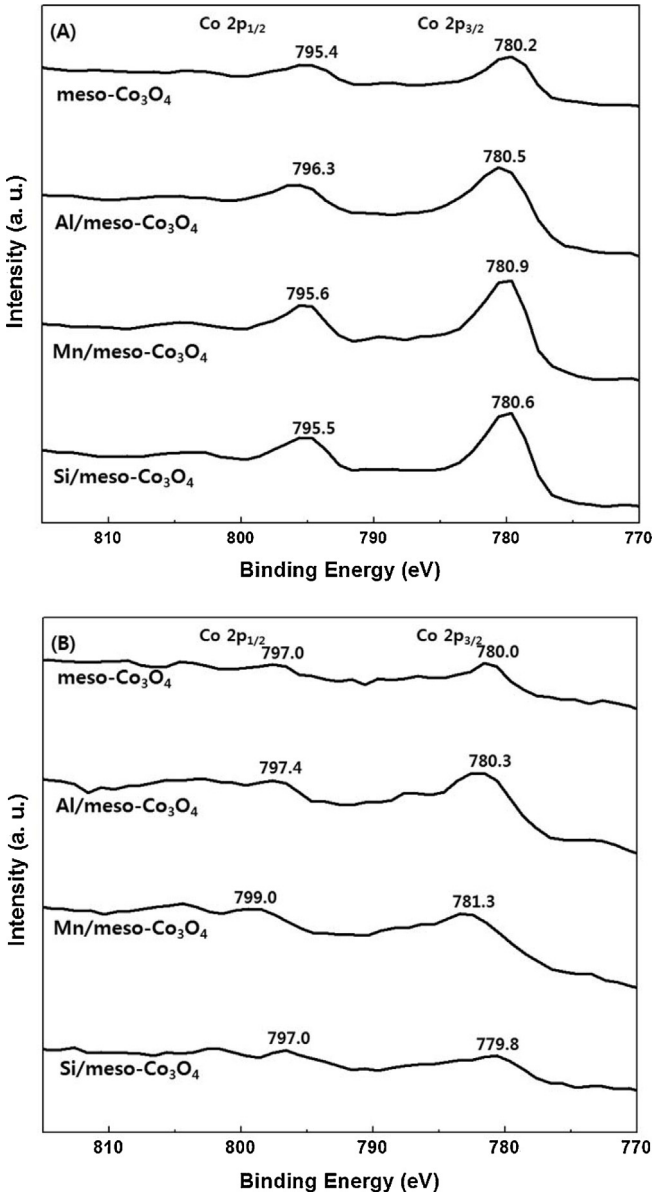

Fig. 8. XPS analysis of Co $2p_{3/2}$ on the fresh and used metal oxide pillared meso-Co_3O_4 catalysts.

The possible coke formation for catalyst deactivation was also verified by characterizing C1s peak through XPS and TGA analysis of the used metal-oxide pillared meso-Co_3O_4. The results of XPS are summarized in the Supplementary Table S1 and Fig. S5. The intensive C1s peaks were observed on all the used catalysts (Fig. S5), however, the deconvoluted peak intensity at the BE of 284.6 eV (Table S1), which can be assigned to graphite or C=C carbons [29,58], was found to be larger on the meso-Co_3O_4 by forming an encapsulated amorphous heavy hydrocarbons on the cobalt particles [24] compared to the Al/meso-Co_3O_4. The larger values of the BEs of above 266 eV on the Mn/meso-Co_3O_4 and Si/meso-Co_3O_4 may be attributed to the presence of hydrocarbons which can be composed of C—O or CC bonds [58], which can be removed hardly under the FTS reaction conditions. Even though the integrated total peak areas of C1s were increased in the order of meso-Co_3O_4 > Al/meso-Co_3O_4 > Si/meso-Co_3O_4 > Mn/meso-Co_3O_4, no significant difference was observed between meso-Co_3O_4 and Al/meso-Co_3O_4. Therefore, the fast catalyst deactivation on the meso-Co_3O_4 can be mainly attributed to the structural collapse of the mesoporous Co_3O_4. In addition, the results of TGA analysis of the used catalysts are shown in Fig. S6. The larger weight loss on the used Al/meso-Co_3O_4 compared to other catalysts was observed below 400 °C, even though it showed a stable catalytic activity. Interestingly, a higher temperature above 400 °C was observed on the meso-Co_3O_4 due to the possible formation of the encapsulated heavy hydrocarbon on the collapsed cobalt particles [24]. The weight gain in the range of 200–400 °C on the Si/meso-Co_3O_4 and meso-Co_3O_4 can be attributed to the reoxidation of metallic cobalt during TGA analysis. Therefore, the coke deposition on the mesoporous cobalt surface seems to be less significant than the structural collapse of metal oxide pillared meso-Co_3O_4.

The FT-IR spectra on the used metal oxide pillared meso-Co_3O_4 displayed in Fig. 9 were collected to further verify the types of deposited hydrocarbons on the outer surfaces of the catalysts. The characteristic CH_2 or CH_3 peaks in the range of wavenumbers in the range of 2800–2950 cm^{-1} can be assigned to the deposited hydrocarbons from polymethylene chains on the metallic cobalt surfaces. The peak at 2920 cm^{-1} (denoted as I_{2920}) can be mainly assigned to asymmetric CH_3 stretching groups from the deposited long-chain hydrocarbons, and the peak at 2850 cm^{-1} (assigned to I_{2850}) can be originated from symmetric stretching of CH_2 groups of polymethylene chains attributed to the relatively short-chain hydrocarbons [54,59,60], which are hardly removable due to strong adsorption

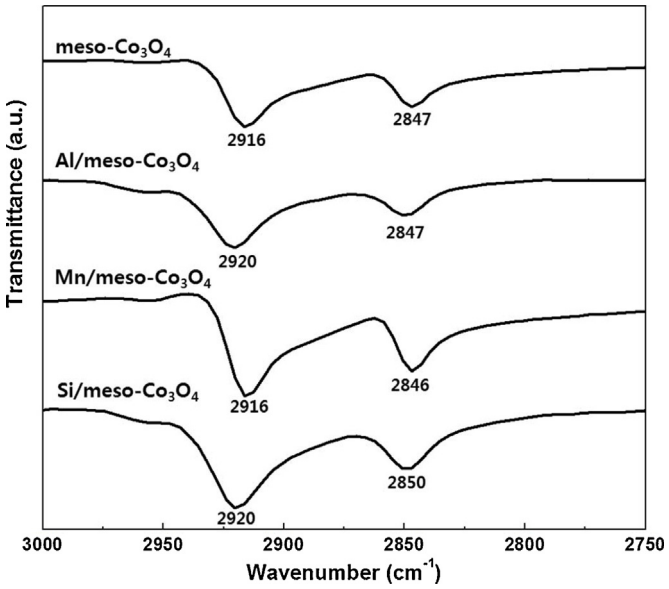

Fig. 9. FT-IR analysis on the used metal oxide pillared meso-Co_3O_4 catalysts.

characters on the cobalt surfaces during the FTS reaction. The observed larger peak intensity of the CH_3 band (larger peak intensity at around 2920 cm^{-1}) on the meso-Co_3O_4 and Mn/meso-Co_3O_4 after the FTS reaction suggests that stronger adsorption characters of amorphous heavier wax components by encapsulating the cobalt surfaces as reported from our previous works [24,34,61]. The peak intensity ratios of I_{2920}/I_{2850}, which represent the integrated area ratios of peak at 2920 cm^{-1} and 2850 cm^{-1}, were also shown in Fig. 9 and Table 3. The values were found to be 1.09, 1.30, 1.15, and 1.19 on the meso-Co_3O_4, Al/meso-Co_3O_4, Mn/meso-Co_3O_4, and meso-Co_3O_4, respectively. We believe that the observed somewhat larger I_{2920}/I_{2850} value on the Al/meso-Co_3O_4 is responsible for a suppressed formation of hardly removal long-chain hydrocarbons, which were also confirmed by the observed lower C_5+ selectivity and TGA analysis. In addition, the observed small peak intensity of the CH_3 band on the Al/meso-Co_3O_4 can reveal the less formation of the heavier hydrocarbons, which can also support the stabilization of catalytic activity of the Al/meso-Co_3O_4 with the help of the Al_2O_3 pillaring metal oxide by increasing structural stability. Even though the Al/meso-Co_3O_4 contained a larger amount of hydrocarbons in the mesopores due to the highest activity among the tested catalysts (results of TGA), these hydrocarbons formed during FTS reaction can be efficiently removed from the ordered stable mesoporous channels of Al/meso-Co_3O_4.

In summary, the structural stability of meso-Co_3O_4 can be enhanced through a simple modification with Al_2O_3 pillaring material even under H_2-rich reductive environment, which can enhance the catalytic activity and stability especially for CO hydrogenation reaction. The role of the Al_2O_3 pillars seems to be to enhance the interactions of the Co_3O_4 surfaces with Al_2O_3 by being highly dispersed inside the regular mesopores, not by forming encapsulated inactive spinel structures. Further optimization of Al/meso-Co_3O_4 remains to be investigated in our laboratory to determine the optimal concentration of Al_2O_3 and proper pretreatment conditions. The Al_2O_3 modification of the meso-Co_3O_4 can effectively stabilize ordered-mesoporous structures even under the reductive environments and the optimized Al/meso-Co_3O_4 catalyst can possibly act as an ordered mesoporous channel reactor by enhancing the transport rates of hydrocarbons formed during the FTS reaction.

4. Conclusions

Ordered mesoporous Co_3O_4 modified with Al_2O_3 pillaring material demonstrated stable and superior catalytic activity even under reductive conditions such as CO hydrogenation reaction to form hydrocarbons. This superior catalytic performance seems to be mainly due to the lower mobility of the Al_2O_3 pillars from forming strong interactions with the surfaces of the mesoporous Co_3O_4. The possible formation of non-reducible inactive cubic $CoAl_2O_4$ spinel structures with strong interactions on the Al/meso-Co_3O_4 may also be responsible for the higher structural stability by maintaining the mesopore structures during the FTS reaction. However, in the case of Mn and Si pillaring materials, the possible formation of MnOx and cobalt silicate can increase the extent of mesopore structure collapse, and subsequently encapsulate the collapsed cobalt particles by simultaneous suppression of syngas transport, resulting in a lower catalytic activity. The ordered-mesoporous structures of Co_3O_4 can also act as an ordered mesoporous channel reactor, which is efficiently working at a higher transport rate of hydrocarbons formed during FTS reaction.

Acknowledgments

This work was supported by the Korea Institute of Energy Technology Evaluation and Planning (KETEP) with Project the number 20132010201750. This work was financially supported by a grant from the Industrial Source Technology Development Programs (2013-10042712) of the Ministry of Knowledge Economy (MKE) of Korea. The authors would like to acknowledge financial support from the National Research Foundation of Korea (NRF) grant funded by the Korean government (NRF-2014R1A1A2A16055557). This work was supported by the National Research Council of Science and Technology (NST) through Degree and Research Center (DRC) Program(2014). This work was also supported by the Korea Institute of Energy Technology Evaluation and Planning (KETEP) under Energy Efficiency and Resources Programs with Project numbers of 20142010102790.

Appendix A. Supplementary data

Supplementary data associated with this article can be found, in the online version, at http://dx.doi.org/10.1016/j.apcatb.2015.06.024

References

[1] B. Ernst, S. Libs, P. Chaumette, A. Kiennemann, Appl. Catal. A: Gen. 186 (1999) 145–168.
[2] A.Y. Khodakov, W. Chu, P. Fongarland, Chem. Rev. 107 (2007) 1692–1744.
[3] D. Vervloet, F. Kapteijn, J. Nijenhuis, J.R. van Ommen, Catal. Sci. Technol. 2 (2012) 1221–1233.
[4] R.J. Madon, E. Iglesia, J. Catal. 139 (1993) 576–590.
[5] D.K. Kim, B.C. Dunn, P. Cole, G. Turpin, R.D. Ernst, R.J. Pugmire, M. Kang, J.M. Kim, E.M. Eyring, Chem. Commun. (2005) 1462–1464.
[6] E. Iglesia, S.L. Soled, R.A. Fiato, J. Catal. 137 (1992) 212–224.
[7] B.G. Johnson, C.H. Batholomew, D.W. Goodman, J. Catal. 128 (1991) 231–247.
[8] T. Tsoncheva, L. Ivanova, J. Rosenholm, M. Linden, Appl. Catal. B: Environ. 89 (2009) 365–374.
[9] I.T. Ghampson, C. Newman, L. Kong, E. Pier, K.D. Hurley, R.A. Pollock, B.R. Walsh, B. Gounde, J. Wright, M.C. Wheeler, R.W. Meulenberg, W.J. DeSisto, B.G. Frederick, R.N. Austin, Appl. Catal. A: Gen. 388 (2010) 57–67.
[10] G. Prieto, A. Martizez, R. Murciano, M.A. Arribas, Appl. Catal. A: Gen. 367 (2009) 146–156.
[11] J.-S. Jung, S.W. Kim, D.J. Moon, Catal. Today 185 (2012) 168–174.
[12] W. Yue, A.H. Hill, A. Harrison, W. Zhou, Chem. Commun. (2007) 2518–2520.
[13] H. Tuysuz, Y. Liu, C. Weidenthaler, F. Schuth, J. Am. Chem. Soc. 130 (2008) 14108–14110.
[14] P. Shu, J. Ruan, C. Gao, H. Li, S. Che, Micropor. Mesopor. Mater. 123 (2009) 314–323.
[15] M. Jin, J.N. Park, J.K. Shon, J.H. Kim, Z. Li, Y.-K. Park, J.M. Kim, Catal. Today 185 (2012) 183–190.

[16] B. Bai, H. Arandiyan, J. Li, Appl. Catal. B: Environ. 142–143 (2013) 677–683.
[17] J. Rosen, G.S. Hutchings, F. Jiao, J. Catal. 310 (2014) 2–9.
[18] Y. Wang, A. Zhu, B. Chen, M. Crocker, C. Shi, Catal. Commun. 36 (2013) 52–57.
[19] Y. Xia, H. Dai, H. Jiang, L. Zhang, Catal. Commun. 11 (2010) 1171–1175.
[20] S. Sun, Q. Gao, H. Wang, J. Zhu, H. Guo, Appl. Catal. B: Environ. 97 (2010) 284–291.
[21] Y. Cui, Z. Wen, S. Sun, Y. Lu, J. Jin, Solid State Ionics 225 (2012) 598–603.
[22] L. Li, Y. Wang, Y. Wang, Y. Han, F. Qiu, G. Liu, C. Yan, D. Song, L. Jiao, H. Yuan, J. Power Source 196 (2011) 10758–10761.
[23] D. Zhao, Y. Wan, W. Zhou, Ordered Mesoporous Materials, Wiley-VCH, 2012.
[24] C. Ahn, H.M. Koo, M. Jin, J.M. Kim, T. Kim, Y. Suh, K.J. Yoon, J.W. Bae, Micropor. Mesopor. Mater. 188 (2014) 196–202.
[25] T. Maiyalagan, A.B.A. Nassr, T.O. Alaje, M. Bron, K. Scott, J. Power Source 211 (2012) 147–153.
[26] T.-W. Kim, F. Kleitz, B. Paul, R. Ryoo, J. Am. Chem. Soc. 127 (2005) 7601–7610.
[27] S. Jun, S.H. Joo, R. Ryoo, M. Kruk, M. Jaroniec, Z. Liu, T. Ohsuna, O. Terasaki, J. Am. Chem. Soc. 122 (2000) 10712–10713.
[28] B.S. Lee, H.M. Koo, M.J. Park, B. Lim, D.J. Moon, K.J. Yoon, J.W. Bae, Catal. Lett. 143 (2013) 18–22.
[29] J.F. Moulder, W.F. Stickle, P.E. Sobol, K.D. Bomben, Handbook of X-ray Photoelectron Spectroscopy, Physical Electronics, Inc., 1995.
[30] H. Zhu, R. Razzaq, L. Jiang, C. Li, Catal. Commun. 23 (2012) 43–47.
[31] H. Xiong, Y. Zhang, K. Liew, J. Li, J. Mol. Catal. A: Chem. 231 (2005) 145–151.
[32] D. Song, J. Li, J. Mol. Catal. A: Chem. 247 (2006) 206–212.
[33] D. Schanke, S. Vada, E.A. Blekkan, A.M. Hilmen, A. Hoff, A. Holmen, J. Catal. 156 (1995) 85–95.
[34] J.W. Bae, S.M. Kim, Y.J. Lee, M.J. Lee, K.W. Jun, Catal. Commun. 10 (2009) 1358–1362.
[35] G. Melaet, W.T. Ralston, C. Li, S. Alayoglu, K. An, N. Musselwhite, B. Kalkan, G.A. Somorjai, J. Am. Chem. Soc. 136 (2014) 2260–2263.
[36] K.S. Smith, Geol. Soc. Am. Rev. Eng. Geol. Volume XVII (2007).
[37] B.A. Sexton, A.E. Hughes, T.W. Turney, J. Catal. 97 (1986) 390–406.
[38] A. Lapidus, A. Krylova, V. Kazanskii, V. Borovkov, A. Zaitsev, J. Rathousky, A. Zukal, M. Jancalkova, Appl. Catal. A 73 (1991) 65–81.
[39] G.L. Bezemer, J.H. Bitter, H.P.C.E. Kuipers, H. Oosterbeek, J.E. Holewijn, X. Xu, F. Kapteijn, A. Jos van Dillen, K.P. de Jong, J. Am. Chem. Soc. 128 (2006) 3956–3964.
[40] J.W. Bae, S.J. Park, M.H. Woo, J.Y. Cheon, K.S. Ha, K.W. Jun, D.H. Lee, H.M. Jung, ChemCatChem 3 (2011) 1342–1347.
[41] I.H. Jang, S.H. Um, B. Lim, M.H. Woo, K.W. Jun, J.B. Lee, J.W. Bae, Appl. Catal. A: Gen. 450 (2013) 88–95.
[42] O. Borg, S. Eri, E.A. Blekkan, S. Storsæter, H. Wigum, E. Rytter, A. Holmen, J. Catal. 248 (2007) 89–100.
[43] A.Y. Khodakov, A. Griboval-Constant, R. Bechara, V.L. Zholobenko, J. Catal. 206 (2002) 230–241.
[44] A.Y. Khodakov, J. Lynch, D. Bazin, B. Rebours, N. Zanier, B. Moisson, P. Chaumette, J. Catal. 168 (1997) 16–25.
[45] P. Munnik, P.E. de Jongh, K.P. de Jong, J. Am. Chem. Soc. 136 (2014) 7333–7340.
[46] E. Rytter, S. Eri, WO 2006/010936 A1 (2006).
[47] J.P. den Breejen, P.B. Radstake, G.L. Bezemer, J.H. Bitter, V. Froseth, A. Holmen, K.P. de Jong, J. Am. Chem. Soc. 131 (2009) 7197–7203.
[48] A. Tuxen, S. Carenco, M. Chintapalli, C.H. Chuang, C. Escudero, E. Pach, P. Jiang, F. Borondics, B. Beberwyck, A.P. Alivisatos, G. Thornton, W.F. Pong, J. Guo, R. Perez, F. Besenbacher, M. Salmeron, J. Am. Chem. Soc. 135 (2013) 2273–2278.
[49] T. Koh, H.M. Koo, T. Yu, B. Lim, J.W. Bae, ACS Catal. 4 (2014) 1054–1060.
[50] S.H. Kwack, M.J. Park, J.W. Bae, S.J. Park, K.S. Ha, K.W. Jun, Fuel Process. Technol. 92 (2011) 2264–2271.
[51] A. Dinse, M. Aigner, M. Ulbrich, G.R. Johnson, A.T. Bell, J. Catal. 288 (2012) 104–114.
[52] T.E. Felters, L. Espinosa-Alfonso, E. de Smit, L. D'souzs, R.J. Meyer, B.M. Weckhuysen, J. Catal. 270 (2010) 95–102.
[53] F. Morales, E. de Smit, F.M.F. de Groot, T. Visser, B.M. Weckhuysen, J. Catal. 246 (2007) 91–99.
[54] J. Aragona, R. Gonzaleza, G. Fuentesb, L. Palinc, G. Crocec, D. Viterbo, Mater. Res. 14 (2011) 25–30.
[55] G. Prieto, P. Concepcion, R. Murciano, A. Martinez, J. Catal. 302 (2013) 37–48.
[56] B. Lee, I.H. Jang, J.W. Bae, S.H. Um, P.J. Yoo, M.J. Park, Y.C. Lee, K.W. Jun, Catal. Surv. Asia 16 (2012) 121–137.
[57] F. Morales, F.M.F. de Groot, O.L.J. Gijzeman, A. Mens, O. Stephan, B.M. Weckhuysen, J. Catal. 230 (2005) 301–308.
[58] Z. Zhao, Y. Dai, G. Ge, Catal. Sci. Technol. 5 (2015) 1548–1557.
[59] J.M.G. Carballo, E. Finocchio, S. Garcıa, S. Rojas, M. Ojeda, G. Busca, J.L.G. Fierro, Catal. Sci. Technol. 1 (2011) 1013–1023.
[60] I. Takahara, K. Murata, K. Sato, Y. Miura, M. Inaba, Y. Liu, Appl. Catal. A: Gen. 450 (2013) 80–87.
[61] S.J. Park, J.W. Bae, G.I. Jung, K.S. Ha, K.W. Jun, Y.J. Lee, H.G. Park, Appl. Catal. A: Gen. 413–414 (2012) 310–321.